BIOCHEMISTRY
including biophysical chemistry & molecular biology
Article

Biochemistry **2010,** *49,* 207–217 207
DOI: 10.1021/bi9017957

Characterization of Thermophilic Archaeal Isopentenyl Phosphate Kinases

Mo Chen[‡] and C. Dale Poulter*

Department of Chemistry, University of Utah, Salt Lake City, Utah 84112 [‡]*Present address: Department of Pharmacology, University of Pennsylvania School of Medicine, 135 John Morgan Building, 3620 Hamilton Walk, Philadelphia, PA 19104-6084*

Received October 19, 2009; Revised Manuscript Received November 22, 2009

ABSTRACT: Archaea synthesize isopentenyl diphosphate (IPP) and dimethylallyl diphosphate (DMAPP), the essential building blocks of isoprenoid compounds, from mevalonate (MVA). However, an analysis of the genomes of several members of the Archaea failed to identify genes for the enzymes required to convert phosphomevalonate (PM) to IPP in eukaryotes. The recent discovery of an isopentenyl kinase (IPK) in *Methanocaldococcus jannaschii* (MJ) suggests a new variation of the MVA pathway where PM is decarboxylated to give isopentenyl phosphate (IP), which is phosphorylated to produce IPP. A blast search using the MJ protein as a probe revealed a subfamily of amino acid kinases that include the fosfomycin resistance protein fomA, which deactivates the antibiotic by phosphorylation of its phosphonate residue in a reaction similar to the conversion of IP to IPP. IPK genes were cloned from two organisms identified in the search, *Methanothermobacter thermautotrophicus* (MTH) and *Thermoplasma acidophilum* (THA), and the His-tagged recombinant proteins were purified by Ni-NTA chromatography. The enzymes catalyze the reversible phosphorylation of IP by ATP, $K_{eq} = 6.3 \pm 1$. The catalytic efficiencies (V/K) of the proteins were $\sim 2 \times 10^6\ M^{-1}\ s^{-1}$. In the reverse direction, ADP was a substrate inhibitor for THA IPK, $K_i^{ADP} = 58 \pm 6\ \mu M$, but not for MTH IPK. Both enzymes were active over a broad range of pH and temperature. Five compounds, dimethylallyl phosphate, isopentenyl thiolophosphate, 1-butyl phosphate, 3-buten-1-yl phosphate, and geranyl phosphate, were evaluated as alternative substrates for the MTH and THA IP kinases. All of the compounds were phosphorylated, although the catalytic efficiency was low for geranyl phosphate.

Isoprenoid molecules comprise the most structurally and chemically diverse family of compounds found in nature (*1*). These molecules are required for life in all organisms except for a few highly symbiotic bacteria with unusually small genomes. While some isoprenoid molecules, for example, ubiquinones, are widely distributed, others are restricted to a specific domain or smaller groups within a domain. The most distinctive chemical markers for members of Archaea are the isoprenoid hydrocarbons found in their membrane lipids. Instead of the fatty acid *sn*-1,2-glyceryl ester motif found in Bacteria and Eukarya, archaeal membrane lipids are *sn*-2,3-glyceryl ethers, where the hydrocarbon chains are derived from C_{20} isoprenoid geranylgeranyl moieties (*2*).

Two pathways are known for the biosynthesis of isopentenyl diphosphate (IPP)[1] and dimethylallyl diphosphate (DMAPP), the fundamental five-carbon building blocks of more complex isoprenoid compounds. The mevalonate (MVA) pathway, discovered in the 1950s, is found in Eukarya, including the cytoplasm of plant cells and a few Bacteria. In these organisms, seven enzymes, acetoacetyl-CoA thiolase, hydroxymethylglutaryl-CoA synthase, hydroxymethylglutaryl-CoA reductase, mevalonate kinase (MVAK), phosphomevalonate kinase (PMK), diphosphomevalonate decarboxylase (DPMD), and IPP isomerase, are required to synthesize IPP and DMAPP from acetate (*3*). The methylerythritol phosphate (MEP) pathway, discovered in the 1990s, is responsible for biosynthesis of IPP and DMAPP from glyceraldehyde phosphate and pyruvate in most Bacteria and in plant chloroplasts. Like Eukarya, Archaea synthesize IPP and DMAPP from MVA. As more archaeal genomes are sequenced and annotated, two genes in the MVA pathway, PMK and DPMD, are often not detected. Although several candidates for archaeal PMK and DPMD in Archaea have been proposed (*4*), only one of the proteins has been characterized biochemically. In that case, the gene product from MJ0044 in *Methanocaldococcus jannaschii*, predicted to be a PMK, was found to be an ATP-dependent kinase for isopentenyl phosphate (IP) (*5*). Whether conversion of PM to IPP is catalyzed by nonorthologous variants of PMK and PPMD that cannot be identified by genomic analysis or some Archaea utilize a modified pathway that bypasses diphosphomevalonate (DPM) is unclear. In other Archaea, homologues of the newly identified gene for IP kinase (IPK) in *M. jannaschii* are colocalized with those genes encoding other

*To whom correspondence should be addressed. Telephone: 801-581-6685. Fax: 801-581-4391. E-mail: poulter@chemistry.utah.edu.

[1]Abbreviations: AAK, amino acid kinase; BP, *n*-butyl phosphate; BPP, *n*-butyl diphosphate; BEP, 3-butenyl phosphate; BEPP, 3-butenyl diphosphate; βME, 2-mercaptoethanol; BSA, bovine serum albumin; DMAP, dimethylallyl phosphate; DMAPP, dimethylallyl diphosphate; DPM, diphosphomevalonate; DPMD, diphosphomevalonate decarboxylase; G6PDH, glucose-6-phosphate dehydrogenase; GP, geranyl phosphate; GPP, geranyl diphosphate; HK, hexokinase; HMG-CoA, 3-hydroxy-3-methylglutaryl-coenzyme A; HRMS, high-resolution mass spectrometry; P_i, inorganic phosphate; IP, isopentenyl phosphate; IPK, isopentenyl phosphate kinase; IPP, isopentenyl diphosphate; ISP, isopentenyl thiolophosphate; ISPP, isopentenyl thiolodiphosphate; LDH, lactate dehydrogenase; MEP, methylerythritol phosphate; MJ, *Methanocaldococcus jannaschii*; MTH, *Methanothermobacter thermautotrophicus*; MVA, mevalonate; MVAK, mevalonate kinase; PEP, phosphoenolpyruvate; PK, pyruvate kinase; PM, phosphomevalonate; PMD, phosphomevalonate decarboxylase; PMK, phosphomevalonate kinase; THA, *Thermoplasma acidophilum*; TMS, tetramethysilane; TEAP, triethylammonium phosphate.

Published on Web 11/23/2009

Scheme 1: Regular and Alternate MVA Pathways for Biosynthesis of IPP

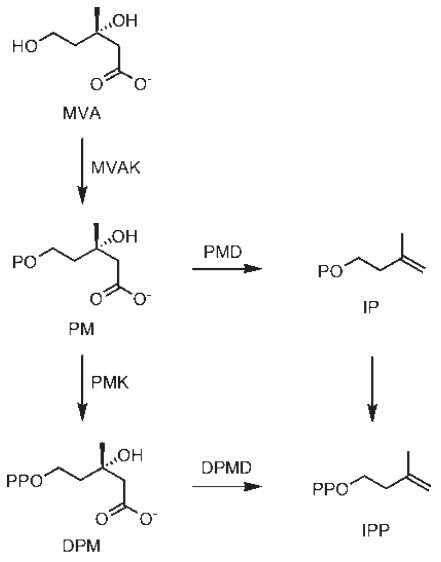

enzymes in the isoprenoid biosynthetic pathway. Grochowski et al. suggested the alternative route for IPP biosynthesis in Archaea that bypasses DPM by an ATP-dependent decarboxylation of PM followed by phosphorylation of IP shown in Scheme 1 (*5*). We now report the characterization of IPKs from *Methanothermobacter thermautotrophicus* and *Thermoplasma acidophilum*.

EXPERIMENTAL PROCEDURES

Materials. [γ-^{32}P]ATP was purchased from PerkinElmer. [1-^{14}C]IPP was purchased from GE Healthcare. Lactate dehydrogenase (rabbit muscle), pyruvate kinase (rabbit muscle), glucose-6-phosphate dehydrogenase (yeast), and hexokinase (yeast) were purchased from Roche. Lactate dehydrogenase (bovine heart) and all other chemicals were from Sigma. IPP was synthesized by Dr. Nicole Heaps, and ISPP was synthesized by Dr. Richard Phan (*6*). Bis(triethylammonium) phosphate (TEAP) was prepared according to the procedure of Keller and Thompson (*7*) and dried over molecular sieves before use. 3-Methyl-3-buten-1-yl *p*-toluenesulfonate (isopentenyl tosylate) was prepared according to the procedure of Davisson et al. (*8*).

3-Methyl-3-buten-1-yl Dimethyl Phosphate. To an ice-cold mixture of 3-methyl-3-buten-1-ol (3.0 g, 35 mmol) and 4-(*N*, *N*-dimethylamino)pyridine (34.0 g, 278 mmol) in 50 mL of CH_2Cl_2 was added dimethyl chlorophosphate (35.2 g, 244 mmol) dropwise by syringe under N_2 (*9*). The mixture was allowed to warm to room temperature and stirred under N_2 overnight. Methanol (10 mL) was added to the mixture, and solvent was removed by rotary evaporation. The resulting white solid was chromatographed on silica gel (from 80:20 to 40:60 v/v hexanes/ethyl acetate), and solvent was removed at reduced pressure to give 5.7 g (84%) of a pale yellow oil: ^{1}H NMR ($CDCl_3$) δ 1.77 (s, 3H), 2.41 (t, 2H, J = 6.8 Hz), 3.75 (s, 3H), 3.79 (s, 3H), 4.78 (dt, 2H, J = 7.4, 6.9 Hz), 4.72 (s, 1H), 4.84 (s, 1H); ^{13}C NMR ($CDCl_3$) δ 22.5, 38.3 (d, J = 7.1 Hz), 54.3 (d, J = 6.1 Hz), 65.9 (d, J = 5.5 Hz), 112.8, 140.9; ^{31}P NMR ($CDCl_3$) δ −0.95; HRMS (MALDI) calcd for $C_7H_{15}O_4P$ [M + H] 195.0781, found 195.0783.

3-Methyl-3-buten-1-yl Phosphate (*Isopentenyl Phosphate, IP*). 3-Methyl-3-buten-1-yl dimethyl phosphate (0.52 g, 2.8 mmol) was treated with 1.3 g (8.5 mmol) of trimethylsilyl bromide in 15 mL of CH_2Cl_2 for 2 h at room temperature (*9*). Methanol (2 mL) was added, and NH_3 was bubbled through the solution to give a white slurry. Solvent was removed by rotary evaporation, and the residue was chromatographed on silica gel (12:5:1 v/v/v 2-propanol/NH_4OH/H_2O). Fractions containing IP, as determined by TLC (12:5:1 v/v/v 2-propanol/NH_4OH/H_2O, R_f = 0.35), were lyophilized to yield 105 mg (20%) of a white solid: ^{1}H NMR (D_2O) δ 1.76 (s, 3H), 2.35 (t, 2H, J = 6.7 Hz), 3.93 (dt, 2H, J = 6.2, 6.7 Hz), 4.82 (s, 1H), 4.85 (s, 1H); ^{13}C NMR (D_2O) δ 22.3, 38.7 (d, J = 7.6 Hz), 63.8 (d, J = 5.0 Hz), 112.1, 144.6; ^{31}P NMR (D_2O) δ 2.13; HRMS (MALDI) calcd for $C_5H_{11}O_4P$ [M − H] 165.0322, found 165.0317.

3-Methyl-3-buten-1-yl Thiolophosphate (*Isopentenyl Thiolophosphate, ISP*). Isopentenyl tosylate (800 mg, 3.3 mmol) was treated with 4.0 g (10 mmol) of tribasic sodium thiophosphate in 160 mL of acetonitrile and 250 mL of H_2O at room temperature for 72 h (*10*). Acetonitrile was removed by rotary evaporation, and H_2O was removed by lyophilization. The residue was chromatographed on silica gel (6:2.5:0.5 v/v/v 2-propanol/NH_4OH/1 M NH_4HCO_3), and solvent was removed as described for the preceding step to yield 275 mg (66%) of a white solid: ^{1}H NMR (D_2O/ND_4OD) δ 1.75 (s, 3H), 2.37 (t, 2H, J = 7.28 Hz), 2.85 (dt, 2H, J = 8.2, 7.4 Hz), 4.79−4.80 (s, 1H), 4.81−4.83 (s, 1H); ^{13}C NMR (D_2O/ND_4OD) δ 21.96, 28.30 (d, J = 2.5 Hz), 38.98 (d, J = 6.6 Hz), 111.30, 146.48; ^{31}P NMR (D_2O/ND_4OD) δ 16.83; HRMS (MALDI) calcd for $C_5H_{11}O_3PS$ [M − H] 181.0094, found 181.0100.

General Procedure for Synthesis of Mono- and Diphosphates by the Cramer Reaction (7). A dry solution of 3.46 g (17.4 mmol) of bis(triethylammonium) phosphate (TEAP) in acetonitrile (15 mL) was added dropwise to a stirred mixture of alcohol (500 mg) in 5 mL of trichloroacetonitrile at room temperature under N_2 in three equal portions with a 5 min interval between each addition (*7*). The mixture was then concentrated at reduced pressure to give a thick dark orange oil. The oil was chromatographed on silica gel (6:2.5:0.5 v/v/v 2-propanol/NH_4OH/H_2O). The fractions were analyzed by silica TLC (6:2.5:0.5 v/v/v 2-propanol/NH_4OH/H_2O), and those containing pure products were combined. Solvent was removed by lyophilization.

3-Methyl-2-buten-1-yl Phosphate (*Dimethylallyl Phosphate, DMAP*). 3-Methyl-2-buten-1-ol (500 mg, 5.8 mmol) was treated with 3.46 g (17.4 mmol) of TEAP. The fractions containing material with an R_f = 0.35 (12:5:1 2-propanol:NH_4OH:water) gave 214 mg (18%) of a white solid: ^{1}H NMR (D_2O) δ 1.71 (s, 3H), 1.76 (s, 3H), 4.35 (dd, 2H, J = 6.9, 6.9 Hz), 5.38−5.45 (m, 1H); ^{13}C NMR (D_2O) δ 17.82, 25.61, 62.79 (d, J = 5.0 Hz), 120.16 (d, J = 7.6 Hz), 140.71; ^{31}P NMR (D_2O) δ 1.17; HRMS (MALDI) calcd for $C_5H_{11}O_4P$ [M − H] 165.0322, found 165.0319.

1-Butyl Phosphate (*BP*) *and 1-Butyl Diphosphate* (*BPP*). *n*-Butanol (500 mg, 6.8 mmol) was treated with 3.46 g (17.4 mmol) of TEAP. The fractions containing material with an R_f = 0.35 (12:1:5 2-propanol:NH_4OH:water) gave 350 mg (28%) BP: ^{1}H NMR (D_2O) δ 0.90 (t, 3H, J = 7.4 Hz), 1.30−1.42 (m, 2H), 1.53−1.62 (m, 2H), 3.80 (dt, 2H, J = 6.3, 6.6 Hz); ^{13}C NMR (D_2O/tBuOH) δ 13.80, 19.10, 32.89 (d, J = 7.1 Hz), 65.67 (d, J = 5.5 Hz); ^{31}P NMR (D_2O) δ 3.18; HRMS (MALDI) calcd for $C_4H_{11}O_4P$ [M − H] 153.0322, found 153.0329.

The fractions containing material with an R_f = 0.13 (12:5:1 2-opropanol:NH_4OH:water) gave 285 mg (22%) of BPP: ^{1}H NMR

(D_2O) δ 0.91 (t, 3H, J = 7.4 Hz), 1.31−1.43 (m, 2H), 1.57−1.66 (m, 2H), 3.93 (dt, 2H, J = 6.7, 6.7 Hz); ^{13}C NMR (D_2O) δ 13.73, 18.94, 32.55 (d, J = 7.1 Hz), 66.87 (d, J = 6.0 Hz); ^{31}P NMR (D_2O) δ −9.99 (d, J = 20.8 Hz), −7.75 (d, J = 20.8 Hz); HRMS (MALDI) calcd for $C_4H_{12}O_7P_2$ [M − H] 232.9986, found 232.9979.

3-Buten-1-yl Phosphate (*BEP*) *and 3-Buten-1-ol*. 3-Buten-1-ol (500 mg, 6.9 mmol) was treated with 3.46 g (17.4 mmol) of TEAP. The fractions containing material with an R_f = 0.35 (12:5:1 2-propanol:NH_4OH:water) gave 355 mg (28%) of BEP: ^{1}H NMR (D_2O) δ 2.38 (dt, 2H, J = 6.7, 6.6 Hz), 3.89 (dt, 2H, J = 6.6, 6.7 Hz), 5.08−5.21 (m, 2H), 5.81−5.95 (m, 1H); ^{13}C NMR (D_2O/tBuOH) δ 34.9 (d, J = 7.1 Hz), 65.2 (d, J = 5.0 Hz), 117.5, 135.8; ^{31}P NMR (D_2O) δ 1.16; HRMS (MALDI) calcd for $C_4H_9O_4P$ [M − H] 151.0166, found 151.0160.

The fractions containing material with an R_f = 0.13 (12:5:1 2-propanol:NH_4OH:water) gave 283 mg (15%) of BEPP: ^{1}H NMR (D_2O) δ 2.41 (dt, 2H, J = 6.7, 6.6 Hz), 3.98 (dt, 2H, J = 6.9, 6.7 Hz), 5.09−5.22 (m, 2H), 5.83−5.97 (m, 1H); ^{13}C NMR (D_2O) δ 34.9 (d, J = 7.1 Hz), 65.8 (d, J = 6.1 Hz), 117.5, 135.8; ^{31}P NMR (D_2O) δ −10.10 (d, J = 20.8 Hz), −7.10 (d, J = 21.4 Hz); HRMS (MALDI) calcd for $C_4H_{10}O_7P_2$ [M − H] 230.9829, found 230.9832.

(*E*)*-3,7-Dimethyl-2,6-octadien-1-yl Phosphate* (*Geranyl Phosphate, GP*). (*E*)-3,7-Dimethyl-2,6-octadien-1-ol (500 mg, 3.25 mmol) was treated with 3.46 g (17.4 mmol) of TEAP. The fractions containing material with an R_f = 0.47 (6:3:1 2-propanol: NH_4OH:water) gave 160 mg (18%) of a white solid: ^{1}H NMR (D_2O) δ 1.59 (s, 3H), 1.66 (s, 3H), 1.69 (s, 3H), 2.02−2.12 (m, 4H), 4.38 (dd, 2H, J = 6.5, 6.6 Hz), 5.14 (t, 1H, J = 6.2 Hz), 5.40 (t, 1H, J = 7.1 Hz); ^{13}C NMR (D_2O/tBuOH) δ 16.3, 17.8, 25.7, 26.6, 39.7, 62.6 (d, J = 5.0 Hz), 120.7 (d, J = 8.6 Hz), 124.8, 132.9, 142.4; ^{31}P NMR (D_2O) δ 1.012; HRMS (MALDI) calcd for $C_{10}H_{19}O_4P$ [M − H] 233.0948, found 233.0941.

Phylogenetic Analysis. IPK homologues (*e*-values lower than 1×10^{-9}) were retrieved by a blastp search against the NCBI nonredundant protein database using the published IPK sequence from *M. jannaschii* DSM 2661 as a query. A phylogenetic tree was built using the PHYLIP package 3.68a according to Boucher et al. (*40*) except the maximum likelihood distance matrix was generated using PROTDIST.

Cloning and Expression. IPK in *M. thermautotrophicus* str. Delta H and *T. acidophilum* DSM 1728 were identified in the blastp search. The IPK gene in MTH (MTH47) was amplified with Easy-A high-fidelity PCR cloning enzyme (Stratagene) from whole cells (ATCC: 29096) using primers 5′-CAT ATG ATC ATT CTC AAG CTT GGT GG-3′ and 5′-GGA TCC ATT AAT GTT TCC CTG TGA TTC TTG-3′. The PCR product was ligated into pGEM-T Easy (Promega) and then subcloned to pET15b (Novagen) using the *Nde*I and *Bam*HI restriction sites to give pET-MTH. The IPK gene in THA (TA0103) was amplified from genomic DNA (ATCC: 25905D) with PfuUltra high-fidelity DNA polymerase (Stratagene) using primers 5′p-TGA TGA TAC TGA AGA TAG GCG GAA G-3′ and 5′-AAA AGC CAA GCT TAT TAT CTT ATC ACC GTA CCT ATG AAT GAT TC-3′. The PCR product was digested with *Hin*dIII and ligated into pET28b (Novagen) prepared by *Nde*I digestion, Pfu polishing, and *Hin*dIII digestion to give plasmid pET-THA. For overexpression, pET-MTH was transformed into Rosetta (DE3) cells (Novagen), and pET-THA was transformed into BL21-(DE3) cells (Novagen), respectively. Overnight cultures were grown, and 30 mL was used to inoculate 1.5 L of LB media supplemented with appropriate antibiotics. The cultures were shaken at 37 °C until OD_{600} ~0.6 followed by addition of IPTG to a final concentration of 1 mM. The induced cultures were incubated at 30 °C for 6 h. Cells were harvested by centrifugation and stored at −80 °C until needed.

Purification. Frozen cell paste was thawed on ice and suspended in lysis buffer (50 mM NaH_2PO_4, pH 8.0, containing 300 mM NaCl and 10 mM imidazole), and cells were disrupted by sonication on ice. DNase I (1 μg/mL) was added to reduce viscosity of the cellular lysate. The crude lysate was centrifuged at 20000 rpm for 20 min. The supernatant was incubated at 50 °C for 10 min, and the precipitated proteins were cleared by centrifugation. The resulting supernatant was incubated with Ni-NTA resin (Qiagen) for 1 h at 4 °C with shaking (110 rpm) and loaded onto a glass fritted column. After the column was washed with lysis buffer and wash buffer (50 mM NaH_2PO_4, pH 8.0, containing 300 mM NaCl and 20 mM imidazole), the protein was eluted with elution buffer (50 mM NaH_2PO_4, pH 8.0, containing 300 mM NaCl and 250 mM imidazole) and analyzed by SDS−PAGE. Fractions containing the pure protein were combined, dialyzed against 20 mM Tris-HCl, pH 8.0, containing 4 mM DTT at 4 °C, and stored in the same buffer with 20% glycerol (v/v) as 100 μL portions at −80 °C.

Mass Spectrometry. Molecular weights of the proteins were determined by direct-infusion positive ion ESI-MS performed on a Waters Micromass Quattro II triple quadrupole mass spectrometer at the Department of Chemistry, University of Utah. Samples were prepared in acetonitrile/H_2O/formic acid (50:50:0.1 v/v/v) with a final protein concentration of 20 pmol/μL.

Oligomeric State of IPK. Size-exclusion chromatography was performed on a Superdex-200 prep grade (GE Healthecare) column (1.3 cm × 25.5 cm, diameter × length) equilibrated using an AKTA-FPLC (GE Healthcare) with 50 mM NaH_2PO_4, pH 7.5, containing 150 mM NaCl at 0.5 mL/min. Ribonuclease A (13.7 kDa), chymotrypsinogen A (25 kDa), ovalbumin (43 kDa), albumin (67 kDa), aldolase (158 kDa), and catalase (232 kDa) (GE Healthecare) were employed as standards. The molecular weight of IPK was calculated from the linear calibration curve according to the manufacturer's protocol.

Product Analysis by Autoradiography. To visualize the turnover of different monophosphate substrates by IPK, 30 nM MTH IPK or 87 nM THA IPK was incubated in the assay buffer (100 mM HEPES, pH 7.5, containing 10 mM $MgCl_2$, 10 mM βME, and 1 mg/mL BSA) containing 1 mM IP, BP, or BEP and 1 mM [γ-^{32}P]ATP at 37 °C for 15, 30, and 60 min. For ISP and DMAP, 3.5 μM MTH IPK or 3.8 μM THA IPK was incubated in the assay buffer containing 2 mM ISP or DMAP and 2 mM [γ-^{32}P]ATP at 37 °C for 15, 30, and 90 min. For GP, 15 μM MTH or THA IPK was incubated in the assay buffer containing 1.5 mM GP and 1 mM [γ-^{32}P]ATP at 37 °C for 15, 30, and 60 min. Multiple parallel controls in the same assay buffer were prepared including samples containing the enzyme only, ATP only, ATP and IPK, or ATP and $HClO_4$. At each time point, 20 μL of the reaction mixture was quenched with 50 μL of methanol/750 mM EDTA (100:13 v/v). Samples (6−8 μL) of the quenched mixture were spotted on silica TLC developed with $CHCl_3$/pyridine/formic acid/H_2O (30:70:16:10 v/v/v/v). The TLC plate was imaged for 24 h using a storage phosphor autoradiography cassette, visualized by a Typhoon 8600 variable mode imager (GE Healthecare), and analyzed using ImageQuant (GE Healthecare).

Product Analysis by NMR. For the forward reaction, 15 μM MTH or THA IPK was incubated in 100 mM HEPES,

pH 7.5, containing 10 mM $MgCl_2$, 10 mM βME, 1 mg/mL BSA, 5 mM IP or the appropriate alternative substrate, and 5 mM ATP, in a final volume of 400 μL at 37 °C for 1 h. After incubation, the reactions were quenched with 10 μL of 750 mM EDTA, and 100 μL of D_2O was added to each sample. The samples containing MTH IPK were spiked with the monophosphate substrate and its expected diphosphate product. The samples containing THA IPK were spiked with ADP and KH_2PO_4 except the one containing DMAP which was spiked with ATP. For the reverse reaction, 15 μM MTH or THA IPK was incubated with 5 mM IPP and 5 mM ADP following the same procedure for the forward reaction. The samples containing MTH IPK were spiked with IP and IPP. The samples containing THA IPK were spiked with ATP and KH_2PO_4. ^{31}P NMR spectra were obtained on the same samples before and after doping.

General Procedure for the Fluorescent Assays. The protocols for fluorescent assays were adopted from Pilloff et al. (*11*) with slight modifications. For both the forward and reverse reactions, IPK was mixed with the assay buffer (100 mM HEPES, pH 7.5, containing 10 mM $MgCl_2$, 10 mM βME, and 1 mg/mL BSA) containing appropriate substrates and coupling enzymes in a final volume of 200 μL to initiate the reaction. The reaction was incubated at 37 °C for 400 s and monitored by the change in fluorescence (λ_{ex} = 340 nm, λ_{em} = 460 nm) (FluoroMax, Jobin Yvon Horiba). Initial rates were measured from the linear portion of the curve (<15% consumption of the concentration-limiting substrate). Kinetic constants were determined by fitting the matrices of initial rates to eq 1 (*12*) using GraFit 5 (Erithacus Software):

$$\frac{v}{[E]} = \frac{k_{cat}[A][B]}{K_d^A K_m^B + K_m^B[A] + K_m^A[B] + [A][B]} \quad (1)$$

where A and B are IP and ATP or IPP and ADP, k_{cat} is the turnover number, K_m is the Michaelis−Menten constant, and K_d is the enzyme−ligand dissociation constant. The coupling enzymes were used without further purification. Their activities were determined in the assay buffer at 33 °C spectrophotometrically. The coupling enzyme concentrations used were to ensure that the system reached 99% of the steady-state rate of the IPK reaction in 45 s (*13*).

Assay for the Forward Reaction. Initial rates for ADP production were determined by monitoring NADH oxidation in a coupled assay with pyruvate kinase (PK) and lactate dehydrogenase (LDH). IPK was incubated in the assay buffer containing 7.7 μM NADH, 1.0 mM phosphoenolpyruvate (PEP), 2.5 units/mL LDH, 3 units/mL PK, and varied concentrations of IP and ATP following the general protocol for the fluorescent assays. For the alternative substrates, IPK was incubated in the assay buffer containing 7.7 μM NADH, 1.0 mM phosphoenolpyruvate, 2.3 units/mL LDH, 4.5 units/mL PK, 200 μM ATP, and varied concentrations of the appropriate alternative substrates.

Assay for the Reverse Reaction. Initial rates for ATP product formation were determined by $NADP^+$ reduction in a coupled assay with hexokinase (HK) and glucose-6-phosphate dehydrogenase (G6PDH). IPK was incubated in the assay buffer containing 0.42 mM $NADP^+$, 1.0 mM glucose, 2.4 units/mL HK, 2 units/mL G6PDH, and varied concentrations of IPP and ADP following the general protocol for the fluorescent assays. The apparent kinetic constants of the reverse reaction of THA IPK were determined using the Michaelis−Menten equation or the modified Michaelis−Menten equation with a term for substrate inhibition.

Equilibrium Constant (K_{eq}). K_{eq} was determined using four different substrate/product mixtures: (1) IP = 500 μM, ATP = 500 μM; (2) IPP = 500 μM, ADP = 500 μM; (3) IP = 250 μM, ATP = 250 μM, IPP = 250 μM, ADP = 250 μM; and (4) IP = 140 μM, ATP = 140 μM, IPP = 360 μM, ADP = 360 μM. The reactions were carried out in 100 mM HEPES, pH 7.5, containing 10 mM $MgCl_2$, 10 mM βME, 1 mg/mL BSA, proper substrate/product mixture, and 2.3 μM MTH IPK or 4.4 μM THA IPK, in a final volume of 500 μL at 37 °C. A 70 μL portion of each sample was quenched with 7 μL of 375 mM EDTA at 30, 60, and 120 min followed by removal of IPK via ultrafitration (Microcon YM-10, Millipore). A 25 μL portion of the filtrate from each sample was transferred to 100 mM HEPES, pH 7.5, containing 20 mM $MgCl_2$, 8 mM βME, 0.8 mg/mL BSA, 1 mM PEP, 0.2 mM NADH, 6.8 units/mL LDH, and 13.6 units/mL PK, in a final volume of 100 μL and incubated at room temperature until there was no further change of absorbance at 340 nm to determine the final concentration of ADP. The equilibrium constant was calculated using eq 2:

$$K_{eq} = \frac{[ADP][IPP]}{[ATP][IP]} \quad (2)$$

where [ADP], [IPP], [ATP], and [IP] are the final concentrations of ADP, IPP, ATP, and IP, respectively. The equilibrium constant for MTH IPK was also calculated from the Haldane relationship (eq 3) (*12*):

$$K_{eq} = \frac{k_{cat}^{forward} K_m^{IPP} K_d^{ADP}}{k_{cat}^{reverse} K_d^{IP} K_m^{ATP}} \quad (3)$$

pH−Activity Profile. A polybuffer composed of 50 mM HEPES, 56 mM MES, and 45 mM CHES was prepared to cover a broad pH range from 5 to 10. The pH of the polybuffer was titrated to pH 10.5 using NaOH and then titrated down to the desired pH at 37 °C using HCl to ensure equal ionic strength at all pH values (*14*, *15*). The activity of the coupling enzymes was determined at different pH values at 33 °C spectrophotometrically. The storage buffers for the coupling enzymes were changed to 5 mM HEPES, pH 6.8, containing 1 mM βME and 1 mg/mL BSA before use by either extensive dialysis or ultrafiltration (Microcon YM-30, Millipore). The pH stability of MTH or THA IPK was evaluated by preincubation at different pH values. The assay for the pH profile was carried out in the polybuffer containing 10 mM $MgCl_2$, 10 mM βME, 1 mg/mL BSA, 100 mM NaCl, 25 μM NADH, 1 mM PEP, 4, 8, or 12 units/mL PK and LDH (depending on the pH), varied concentrations of IP, and 2.4 mM ATP, in a final volume of 200 μL at 37 °C. Initial rates were determined using the fluorescent assays following the general protocol and fit to the Michaelis−Menten equation to obtain k_{cat}^{IP} and k_{cat}^{IP}/K_m^{IP}. The pK_a values of the pH profile were obtained by fitting k_{cat}^{IP} and k_{cat}^{IP}/K_m^{IP} to a bell-shaped curve described by eq 4 (*16*),

$$Y = \frac{Y_{lim}}{1 + 10^{pK_1 - pH} + 10^{pH - pK_2}} \quad (4)$$

where Y is k_{cat}^{IP} or k_{cat}^{IP}/K_m^{IP}, Y_{lim} is the limiting value of the curve at neutral pH, and K_1 and K_2 are the molecular dissociation constants for the acidic and basic limbs, respectively.

Temperature−Activity Profile. The stability of IPK versus temperature was evaluated by preincubation of the enzyme in

5 mM HEPES buffer, pH 7.5, containing 1 mg/mL BSA at different temperatures for 10 min. The remaining activity was determined by diluting the enzyme 10-fold into 100 mM HEPES buffer, pH 7.5, containing 10 mM $MgCl_2$, 10 mM βME, 1 mg/mL BSA, 1 mM PEP, 150 μM NADH, 6.25 units/mL LDH, 7.5 units/mL PK, 200 μM IP, and 200 μM ATP, in a final volume of 100 μL at 37 °C with the absorbance change monitored at 340 nm. For the temperature profile, MTH or THA IPK was incubated in 136 mM HEPES, pH 7.5, containing 10 mM $MgCl_2$, 10 mM βME, 1 mg/mL BSA, 1 mM IP, and 1 mM ATP, in a final volume of 50 μL at different temperatures for 10 min and then quenched with 5 μL of 375 mM EDTA. IPK was removed via ultrafiltration (Microcon YM-10, Millipore). The activity of IPK was calculated from the ADP concentration in the filtrate determined following the same procedure used for the equilibrium constant determination.

RESULTS

Genetic Correlations. A blastp search against the NCBI nonredundant protein database using MJ IPK as a query retrieved 107 sequences for proteins with *e*-values lower than $<10^{-9}$ (Supporting Information Table S1). In this group, 5 are annotated as IP kinases. Except for 2 fosfomycin kinases, the rest are members of the amino acid kinase family. Thus, MJ IPK clusters with proteins in the amino acid kinase (AAK) superfamily, which resemble those in the FomA-like subfamily. FomA is a resistance protein in fosfomycin-producing strains of *Streptomyces* that inactivates the antibiotic by phosphorylation of its phosphonate moiety in a reaction similar to that for the conversion of IP to IPP. The two other kinases in the MVA pathway, mevalonate kinase and PMK, belong to the GHMP kinase superfamily (*17*). Of the 107 AAK proteins, 78 are from Archaea representing 21 different families within the kingdom, 21 from Eukarya, and 8 from Bacteria. The archaeal proteins in this group most distant from MJ IPK are from *T. acidophilum* ($7e^{-13}$) and *Picrophilus torridus* ($3e^{-12}$) (see Figure 1).

Sequence alignments for the AAK proteins from Bacteria, Eukarya, 13 different families of Archaea, and the fomA proteins from *Streptomyces* show a pattern of highly conserved motifs corresponding to amino acids identified in the X-ray structure of *Streptomyces wedmorensis* fomA that are important for binding the phosphate in fosfomycin (blue squares), the phosphate residues in ATP (red squares), the adenosine nucleoside (orange squares), and a histidine (purple square) implicated in catalysis (Supporting Information Table S2). Thus, it appears that the basic catalytic machinery utilized by fomA to catalyze the ATP-dependent phosphorylation of fosfomycin is found in all of the proteins identified in our blast search.

Expression, Purification, and Molecular Mass. Two proteins from the blast search were selected for characterization. One, from *M. thermautotrophicus* (MTH), shows high overall similarity to the MJ enzyme ($3e^{-29}$), while the other, from *T. acidophilum* (THA), is more distant ($2e^{-13}$). Recombinant N-terminal His-tagged MTH and THA IPKs were expressed in *Escherichia coli* and purified by a combination of heat treatment and Ni-NTA chromatography. Positive ion ESI-MS gave a molecular mass of 31118 and 29084 Da for the MTH and THA proteins, respectively. These values agreed well with the calculated masses of 31116 and 29082 Da. Their respective molecular masses determined by size-exclusion chromatography were 69 ± 2 and 51.8 ± 0.7 kDa, indicating that both proteins are homodimers. This is consistent with the most common observed oligomeric state of other members of the AAK family (*18*−*21*). Dimer formation is believed to be important for catalysis by providing a scaffold that anchors loops surrounding the substrate binding site (*22*, *23*). Both MTH and THA IPKs are prone to aggregation at moderate concentrations (> 10 mg/mL).

Product Analysis. The MTH and THA proteins were incubated with ATP and IP and with ADP and IPP. Products of the reactions were analyzed by ^{31}P NMR spectroscopy, and the spectra are shown in Figures 2 and 3. ^{31}P resonances for MTH IPK (Figure 2, black) are clearly resolved for IP (singlet, 3.7 ppm), IPP (P_α, doublet, −10.1 ppm; P_β, doublet, −6.4 ppm), ATP (P_α, doublet, −10.7 ppm; P_β, doublet, −5.9 ppm, P_γ, triplet, −21.4 ppm). Addition of IP and IPP selectively increased the intensity of the peaks for the IP and IPP resonances (red). A similar spectrum was seen for THA IPK in Figure 3 (black), and addition of ATP selectively increased the intensity of the α, β, and γ signals (red). A small peak at 2.6 ppm was attributed to P_i contamination in the enzyme storage buffer and was enhanced upon addition of K_2HPO_4 to the sample (red). These observations are similar to those reported for MJ IPK (*5*). The NMR spectra clearly indicate that both enzymes catalyze the interconversion of IP/ATP and IPP/ADP. Quantitatively, the conversion of IP to IPP approximately equaled the conversion of ATP to ADP, judged by the intensity of the corresponding peaks or vice versa. Thus, the proteins can be classified as IP kinases along with the MJ enzyme.

Kinetic Constants. Initial rates for the forward reaction were determined by an assay where ADP production was coupled to consumption of NADH. Many kinases possess intrinsic ATPase activity (*24*−*29*). While the rate of the ATPase reaction is typically negligible (*30*), it can be sufficiently large to interfere with measurements of the kinase activity in some cases (*26*, *31*). We screened both enzymes for ATPase activity by a TLC-based assay using [γ-^{32}P]ATP and found that their intrinsic ATPase activity was negligible relative to their kinase activity (data not shown). Initial rates were determined at four to seven concentrations of ATP and IP covering the range from $0.5K_m$ to $10K_m$. Lineweaver−Burk plots of the initial rates were obtained by varying ATP concentrations while fixing IP concentration (Figure 4A,B). The plots for both MTH and THA IPKs showed the same pattern: a family of lines intersecting in quadrant II. This pattern is best described by a sequential mechanism. The kinetic constants were obtained using eq 1 (Table 1). Values for K_d were obtained by substituting [IPP] for [A] and [ATP] for [B] and vice versa.

The kinetic analyses of the reverse reaction were performed using a fluorescent assay where ATP production was coupled with the generation of NADPH. For MTH IPK, the matrix of initial rates determined at four different concentrations of each substrate covering the range from K_m to $5K_m$. The plots obtained from MTH IPK at varied ADP concentrations while fixing the IPP concentration indicate a sequential mechanism, as for the forward reaction (Figure 4C, Table 1). While substrate inhibition by ADP was not seen for MTH IPK up to nucleotide concentrations of 150 μM, it was seen for ADP concentrations as low as 20 μM for the reverse reaction of THA IPK. Attempts to determine the kinetic parameters for the reverse reaction of THA IPK were limited by the detection limits of the assay, which requires substrate concentrations greater than 5 μM, about two times of the K_ms of THA IPK. As a result, apparent values for K_m^{ADP} and K_i^{ADP} were determined at a saturating IPP concentration, and an

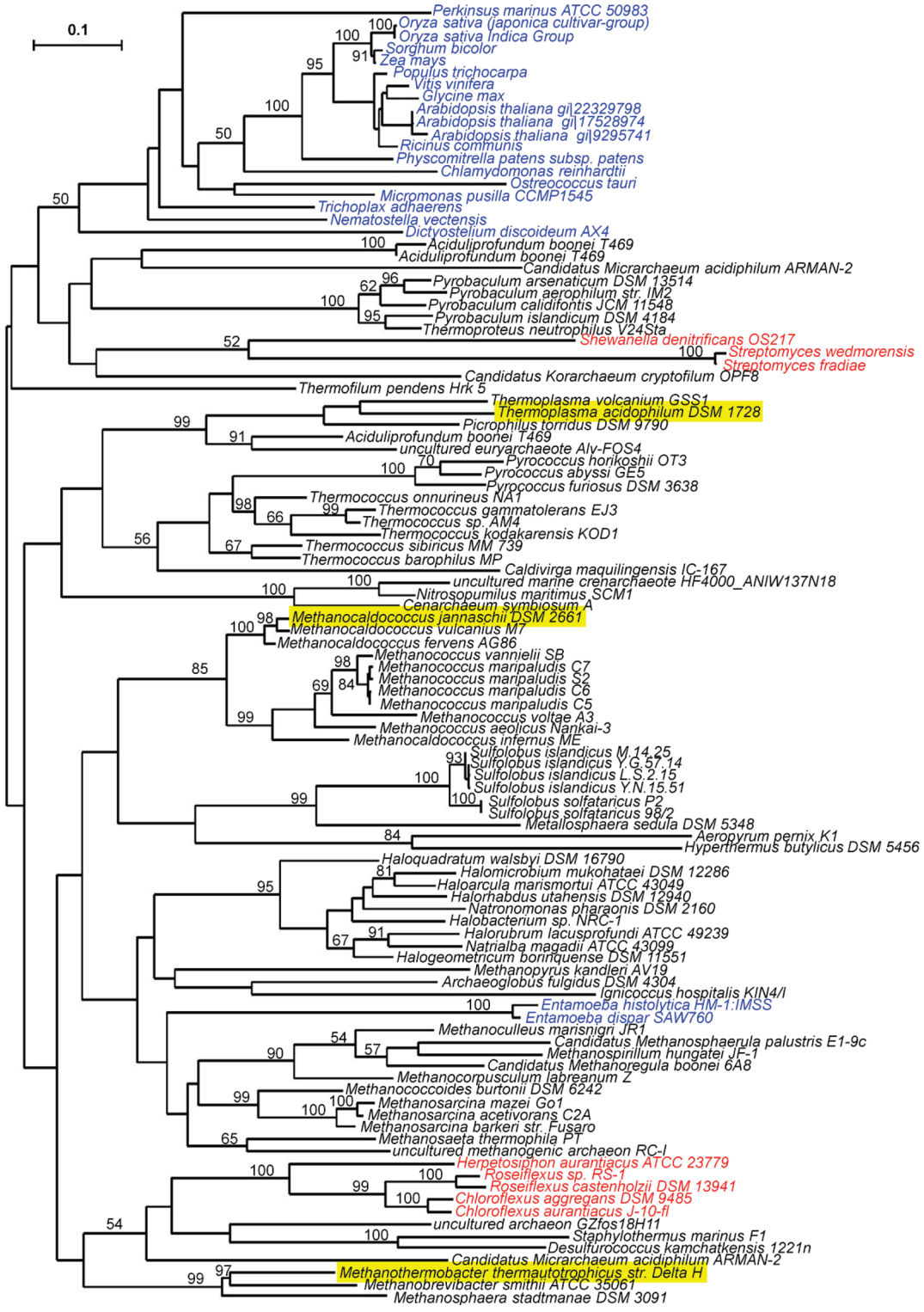

FIGURE 1: Best maximum likelihood phylogenetic tree for IPK homologues. Sequences from Archaea (black), Eukaryota (blue), and Bacteria (red). IPKs characterized are underlined. Bootstrap values are not shown where the bootstrap consensus tree disagreed with the best tree or values are less than 50. The tree is unrooted.

apparent K_m^{IPP} was determined at the ADP concentration where the maximum activity was observed (Table 1).

Equilibrium Constant. High concentrations of the IPKs were incubated with substrate/product mixtures at 37 °C. Equilibrium was reached within 30 min. The equilibrium constant (K_{eq}) for the reaction was calculated from eq 2 to give values of 6.5 ± 0.4 and 6.2 ± 1.1 for data from MTH IPK and THA IPK, respectively. A value for K_{eq} calculated using the Haldane relationship (eq 3) and the kinetic parameters in Table 1 was 11.3.

pH−Activity Profile. The pH dependence of the kinetic constants for IP in the forward reaction was determined at a saturating ATP concentration. Assays were performed within the range of pHs where the IPKs were stable. The initial rates of the reactions were determined via the coupled fluorescent assay. Higher NADH concentrations were used in the assays

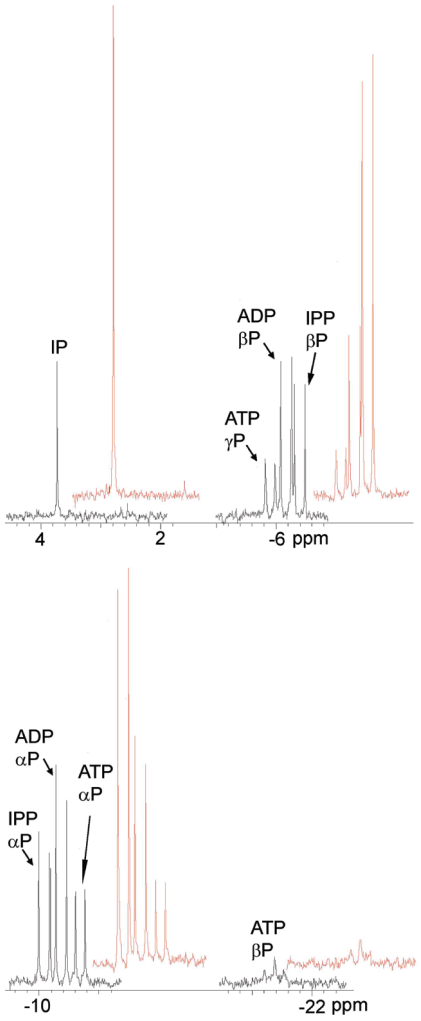

FIGURE 2: ^{31}P NMR spectra after incubation of MTH IPK with IP and ATP (black) and after addition of IP and IPP (red).

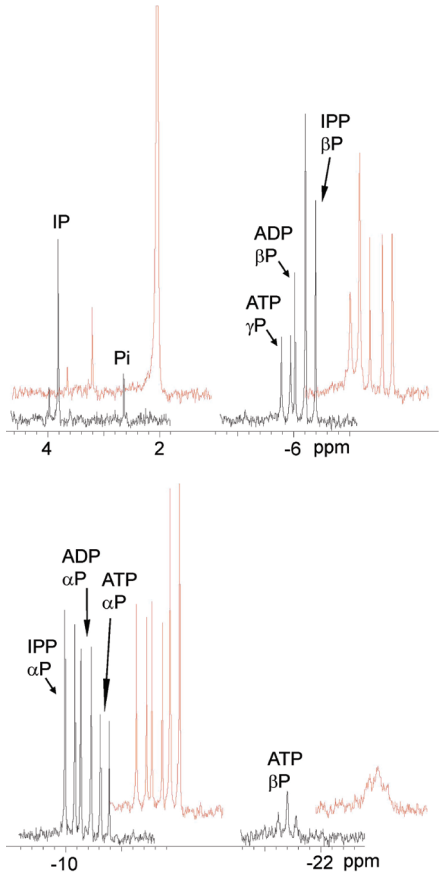

FIGURE 3: ^{31}P NMR spectra after incubation of THA IPK with IPP and ADP (black) and after addition of ATP and K_2HPO_4 (red). The sample showed a small peak for inorganic phosphate (P_i) before the additions.

to compensate pronounced nonenzymatic ATP hydrolysis at extreme pH values.

For MTH IPK, the k_{cat}^{IP}/K_m^{IP} data gave a standard bell-shaped curve (Figure 5A). The k_{cat}^{IP} was independent of pH from pH 6.80 to pH 9.72 (Figure 5B). The pK_a of the acidic limb (pK_1) was 6.7 ± 0.1, and the pK_a of the basic limb (pK_2) was 9.9 ± 0.1 with a maximal value $k_{cat}^{IP}/K_m^{IP} = 1.31 \pm 0.05\ \mu M^{-1}\ s^{-1}$. The pH profiles for k_{cat}^{IP}/K_m^{IP} and k_{cat}^{IP} for THA IPK were bell-shaped (Figure 5C,D). The pK_a values for the k_{cat}^{IP}/K_m^{IP}−pH profile were pK_1 = 6.5 ± 0.1 and pK_2 = 8.5 ± 0.2 with a maximal value $k_{cat}^{IP}/K_m^{IP} = 1.1 \pm 0.1\ \mu M^{-1}\ s^{-1}$. Those for the k_{cat}^{IP}−pH profile were pK_1 = 5.7 ± 0.1 and pK_2 = 8.8 ± 0.2 with a maximal value $k_{cat}^{IP} = 12.1 \pm 0.6\ s^{-1}$.

Temperature−Activity Profile. A preliminary temperature−activity profile for MTH and THA IPK was determined using a 10 min end-point assay at fixed substrate concentrations to avoid the denaturation of the coupling enzymes at high temperatures (Figure 6). Preliminary experiments indicated that MTH IPK was stable up to 50 °C and THA IPK was stable up to 70 °C. Above these temperatures, the profile reflects a combination of the temperature-dependent increase in activity and enzyme denaturation. Nevertheless, the initial rates for both MTH and THA IPKs increased to maximum values at 70 °C and then decreased at higher temperatures under the current assay conditions.

Alternate Substrates. Five compounds, dimethylallyl phosphate (DMAP), isopentenyl thiolophosphate (ISP), 1-butyl phosphate (BP), 3-buten-1-yl phosphate (BEP), and geranyl phosphate (GP), were evaluated as alternative substrates for the MTH and THA IP kinases (Figure 7). Turnover was detected by incubating IPK with the alternate substrates and [γ-^{32}P]ATP. Following incubation, the reaction mixtures were separated by TLC and analyzed by storage phosphor autoradiography (Figure 8). It is clear from the autoradiographs that both MTH (part A) and THA (part B) IPKs catalyze phosphorylation of all of the alternative substrates we evaluated, although the slow turnover rate of GP required higher enzyme concentrations to give detectable amounts of GPP within the same incubation period. There was a small amount of an unidentified radioactive species with an R_f value similar to that of IPP visible in most the samples. This spot appears to be from inorganic phosphate generated by the degradation of [γ-^{32}P]ATP, as demonstrated in the control sample (C2) where ATP was treated with acid. More intense spots for inorganic phosphate were observed during phosphorylation of GP. Formation of P_i resulted from low-level ATPase activity (about one-thousandth of the kinase activity) that was enhanced at high enzyme concentration and did not depend on GP concentration in time course experiments (data not shown).

Steady-state kinetic constants for the substrate analogues are shown in Table 2. The analogues with small hydrocarbon moieties were all good substrates for the IPKs, although there were relatively minor variations in the activities of MTH and

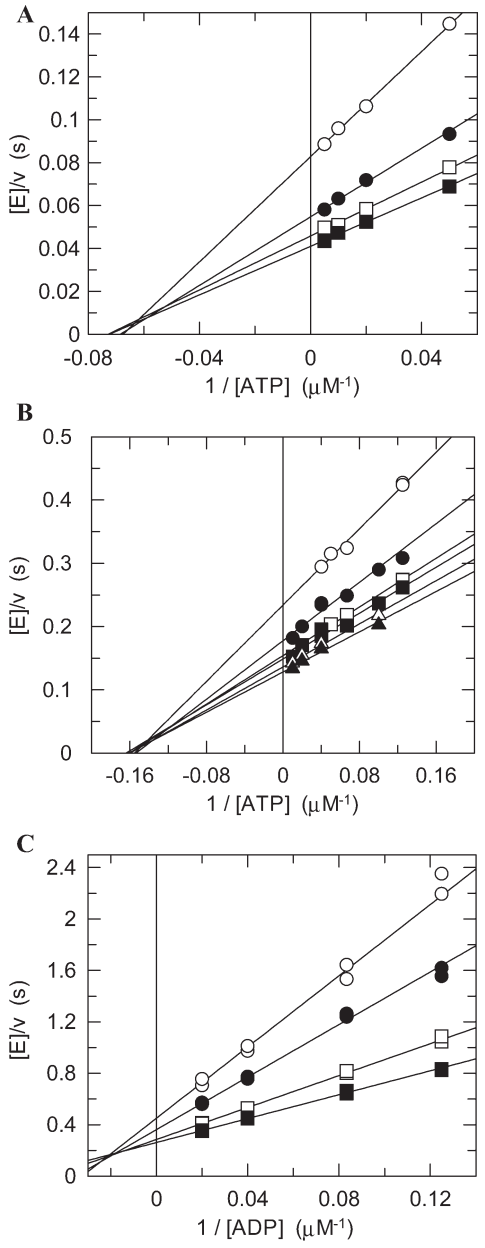

FIGURE 4: Steady-state kinetic analysis. Part A: MTH IPK for the forward reaction using ATP as the varied substrate. IP concentrations: 10 μM (○), 25 μM (●), 50 μM (□), and 100 μM (■). Part B: THA IPK for the forward reaction using ATP as the varied substrate. IP concentrations: 5 μM (○), 10 μM (●), 15 μM (□), 25 μM (■), 50 μM (●), and 100 μM (▲). Part C: MTH IPK for the reverse reaction using ADP as the varied substrate. IPP concentrations: 8 μM (○), 12 μM (●), 25 μM (□), and 50 μM (■).

THA IPK for the individual compounds. Most of the decrease in catalytic efficiency (V/K) for these analogues results from higher K_m values relative to IP. Based on these results, it is likely that the enzymes will accept a variety of small organic phosphates as substrates. GP is only marginally active, even at high enzyme concentrations. The low catalytic efficiency for this substrate results from unfavorable changes in k_{cat} and K_m, probably as a result of crowding in the active site due to the large geranyl moiety.

The identities of the products were confirmed by NMR spectroscopy as described for the normal substrates (Figures 1S−5S, Supporting Information). The production of the corresponding diphosphates could be observed for ISP, DMAP, BP,

Table 1: Steady-State Kinetic Constants for IPKs

enzyme	substrate	k_{cat} (s^{-1})	K_m (μM)	K_d (μM)	k_{cat}/K_m (M^{-1} s^{-1})
MTH IPK	IP	27.5 ± 0.3	12.7 ± 0.6	15.3 ± 2.6	2.2×10^6
	ATP		13.4 ± 0.8	16.2 ± 2.5	2.2×10^6
	IPP	4.5 ± 0.1	7.6 ± 0.8	29.4 ± 2.9	5.9×10^5
	ADP		13.0 ± 1.0	50.2 ± 6.4	3.4×10^5
THA IPK	IP	8.0 ± 0.2	4.4 ± 0.5	4.6 ± 1.5	1.8×10^6
	ATP		6.0 ± 0.5	6.3 ± 2.2	1.3×10^6
	IPP[a]	2.75 ± 0.03	2.7 ± 0.2		1.0×10^6
	ADP[b]	3.6 ± 0.1	3.1 ± 0.4	57.9 ± 5.8[c]	1.2×10^6

[a]Apparent kinetic constant determined at ADP = 12 μM. [b]Apparent kinetic constant determined at IPP = 80 μM. [c]Substrate inhibition constant K_i (μM).

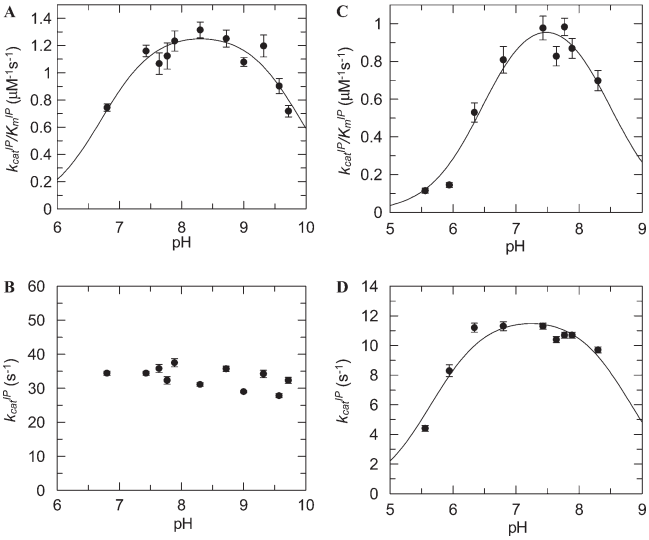

FIGURE 5: pH−activity profiles of MTH IPK. (A) k_{cat}^{IP}/K_m^{IP}−pH profile with pK_a values of 6.7 ± 0.1 and 9.9 ± 0.1. (B) k_{cat}^{IP}−pH profile. pH−activity profiles of THA IPK. (C) k_{cat}^{IP}/K_m^{IP}−pH profile with pK_a values of 6.5 ± 0.1 and 8.5 ± 0.2. (D) k_{cat}^{IP}−pH profile with pK_a values of 5.7 ± 0.1 and 8.8 ± 0.2.

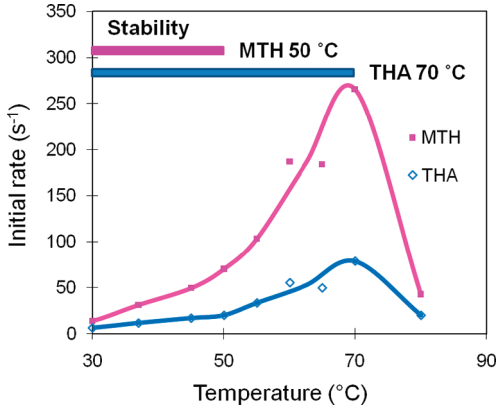

FIGURE 6: Temperature−activity profiles of MTH IPK (■) and THA IPK (●). MTH IPK is stable until 50 °C, and THA IPK is stable until 70 °C.

and BEP for both MTH and THA IPKs and for GP with MTH IPK. Although trace amounts of GPP were seen in incubations of GP and ATP with THA IPK by autoradiography (Figure 8B), no peaks corresponding to the product were observed in the ^{31}P spectrum of the mixture. However, peaks were seen for ADP

produced by the competing ATPase activity. A significant amount of P_i was detected in the incubations with ISP, which was not observed in the radioactive assays. Control experiments confirmed that ISP slowly hydrolyzed at neutral pH in buffer without enzyme (data not shown).

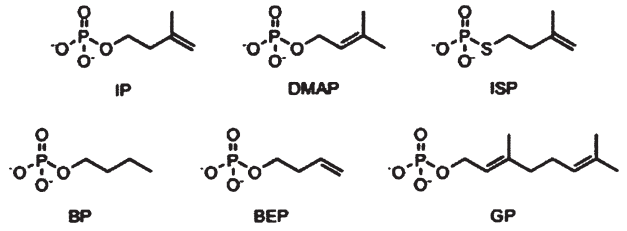

FIGURE 7: Substrate analogues for MTH and THA IPK.

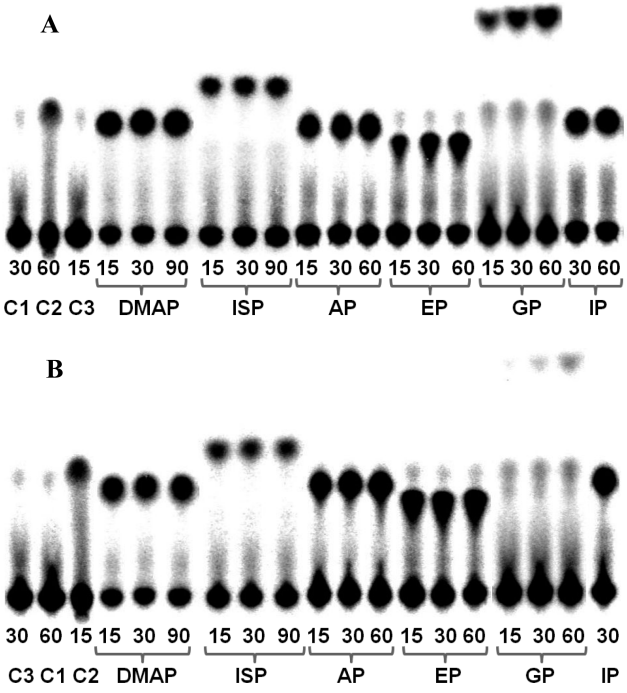

FIGURE 8: TLC analysis of incubations of MTH IPK (A) and THA IPK (B) with IP and alternative substrates DMAP, ISP, BP, BEP, and GP. C1, C2, and C3 were the following controls: C1, ATP; C2, [γ-^{32}P]ATP after acidic hydrolysis to give [γ-^{32}P]P_i; C3, ATP and IPK. Incubation time (min) is indicated below each lane.

DISCUSSION

A search of the NCBI database using MJ IPK as a probe identified a large group of proteins described as fomA-like proteins in the AAK superfamily. The majority of the hits with *e*-values below −10 were from Archaea with representatives from 21 different families in the kingdom. Hits were also found in a few Bacteria, including fomA from *S. wedmorensis* ($4e^{-10}$), and Eukarya. A multiple sequence alignment of the 107 proteins from MJ IPK to *S. wedmorensis* fomA revealed several conserved regions. Notably, those residues identified in the catalytic site of the crystal structure of fomA important for substrate binding and catalysis are preserved in most of the sequences. Thus, it is likely that this group of proteins catalyzes the ATP-dependent phosphorylation of similar substrates.

We selected two proteins from the list, a hypothetical protein from *M. thermautotrophicus* with substantial homology to MJ IPK ($5e^{-29}$) and a more distantly related γ-glutamyl kinase related protein from *T. acidophilum* ($7e^{-13}$), for further study. Like the fomA protein, the *M. thermautotrophicus* and *T. acidophilum* proteins are homodimers. Both catalyze the reversible ATP-dependent phosphorylation of IP. *In vivo*, the phosphorylation of IP is likely heavily preferred, driven by low ADP concentrations in the cell and efficient removal of IPP by the irreversible downstream chain elongation reactions. Although k_{cat} and K_m for MJ IPK measured at 55 °C are ~10-fold higher than the values listed in Table 1 (*5*), which we measured at 37 °C, the catalytic efficiencies (V/K) of three proteins are similar. Values for $V/K \approx 10^6\ s^{-1}\ M^{-1}$ are consistent with those typically found for biosynthetic enzymes.

IP kinase activity is associated with a variant of the MVA pathway in Archaea (Scheme 1), where PM is decarboxylated to give IP, which is then phosphorylated to produce IPP. Although labeling studies clearly establish that MVA is efficiently incorporated into isoprenoid compounds in Archaea, there are elements of uncertainty at this point about how MVA is converted to IPP. Activity for a putative PMD has not been firmly established, and IPK homologues are found in several strains from *Halobacterium*, *Thermoplasma*, and *Sulfolobus* thought to contain DPMD or DPMD and PMK. The occurrence of IPK homologues in many different families of Archaea suggests that a route from MVA involving conversion of IP to IPP is the dominant pathway for isoprenoid biosynthesis in these organisms.

Kinetic analyses indicate sequential mechanisms for the forward reactions catalyzed by MTH and THA IPK and for the

Table 2: Apparent Kinetic Constants with Alternate Substrates[a]

enzyme	substrate	k_{cat} (s^{-1})	K_m (μM)	k_{cat}/K_m ($M^{-1}\ s^{-1}$)	relative k_{cat}/K_m (%)
MTH IPK	IP[b]	27.5 ± 0.3	12.7 ± 0.6	2.2×10^6	100
	ISP	8.22 ± 0.09	23.7 ± 0.8	3.5×10^5	16
	DMAP	34.0 ± 0.3	43.2 ± 1.0	7.9×10^5	36
	BP	31.8 ± 0.7	263 ± 18	1.2×10^5	5.5
	BEP	20.5 ± 0.3	297 ± 12	6.9×10^4	3.1
	GP	0.0142 ± 0.0002	740 ± 43	19	0.00086
THA IPK	IP[b]	8.0 ± 0.2	4.4 ± 0.5	1.8×10^6	100
	ISP	2.84 ± 0.06	14.5 ± 1.2	2.0×10^5	11
	DMAP	11.3 ± 0.4	174 ± 18	6.5×10^4	3.6
	BP	9.9 ± 0.1	173 ± 7	5.7×10^4	3.2
	BEP	8.07 ± 0.09	103 ± 5	7.8×10^4	4.3
	GP[c]	0.047 ± 0.008	4700 ± 1300	10	0.00055

[a]Apparent kinetic constants determined at ATP = 200 μM. [b]Data from reference (the characterization paper). [c]The highest GP concentration used was 4.5 mM.

reverse reaction of MTH IPK. These results are consistent with a single displacement mechanism for phosphoryl transfer, without the intervention of phosphoryl-enzyme intermediate. Other AAK family members catalyze phosphorylation by sequential mechanisms, which can be either ordered or random (*32*−*36*). Our results do not permit us to distinguish between ordered and random mechanisms for MHT and THA IPK.

The MTH and THA IPKs are very stable below 50 °C and are active over a broad pH range. MTH IPK prefers alkaline conditions, while THA IPK prefers acidic conditions. The k_{cat}^{IP} values of MTH IPK are independent of pH, suggesting a single rate-limiting step with the same protonation state of the enzyme−substrate complex throughout the entire tested pH range. The k_{cat}^{IP}/K_m^{IP} pH−activity profile is bell-shaped with $pK_1 = 6.7 \pm 0.1$ for the acidic limb and $pK_2 = 9.9 \pm 0.1$ for the basic limb. pK_a values of IP were not found in the literature. However, pK_as for related alkyl phosphates, including methyl, ethyl, *n*-propyl, and *n*-butyl phosphate, are less than 2.0 for the dissociation of the first proton and between 6.3 and 6.9 for the dissociation of the second proton (*37*). The $pK_1 = 6.7$ for the k_{cat}^{IP}/K_m^{IP}−pH profile of MTH IPK could correspond to the dissociation of the second proton in IP or protonation of an imidazole ring in histidine ($pK_a = 6.3$ at 25 °C) (*38*). Sequence alignments show that MTH IPK has a conserved histidine found in the active site of the homologous fomA protein. The acidic limb of the profile may reflect a combination of overlapping titration curves for the substrate and the active site histidine. $pK_2 = 9.9$ for MTH IPK does not correlate with a pK_a for the substrate and likely reflects ionization of a residue in the enzyme, probably a tyrosine (pK_a 9.6 at 25 °C) based on the likely location of tyrosine residues in the active site based on fomA structure. Both the k_{cat}^{IP} and the k_{cat}^{IP}/K_m^{IP} pH−activity profiles for THA IPK are bell-shaped. This suggests multiple ionization states for the THA IPK−substrate complex over the range of pHs examined. $pK_1 = 6.5 \pm 0.1$ for the k_{cat}^{IP}/K_m^{IP} pH−activity profile and $pK_2 = 8.5 \pm 0.2$. The value for pK_1 is similar to that for MTH IPK. The value for pK_2 probably reflects ionization of an amino acid side chain. However, the structural model based on fomA rules out a cysteine (pK_a 8.3 at 25 °C) (*38*), and presumably the pK_a of another ionizable residue has shifted to this range.

MTH and THA IPK phosphoryate a variety of small C_4 and C_5 organic phosphates. These molecules are good substrates with k_{cat}s similar to k_{cat}^{IP} and only somewhat elevated K_ms. Incubation of these substrates with [γ-^{32}P]ATP provides a convenient approach for obtaining ^{32}P-labeled molecules whose synthesis by chemical procedures would be difficult. GP, in contrast, is a poor substrate with a substantially lower k_{cat} and a higher K_m. The size of the binding pocket appears too small to accommodate the C_{10} substrate, and the weakly bound substrate is apparently not aligned optimally for catalysis.

In conclusion, a blast search using MJ IPK as a probe revealed a large family of putative IP kinases in Archaea, along with a few homologues in Eukarya and Bacteria, including the fomA fosfomycin resistance proteins in *S. wedmorensis* and *Streptomyces fradiae*. The IP kinases have strong homology to fomA, including several highly conserved residues located in the active site of fomA. The IP kinases transfer the γ-phosphate in ATP to the phosphate moiety in IP, while fomA inactivates fosfomycin by an ATP-dependent phosphorylation of the phosphonate moiety in the antibiotic. Because of the wide distribution of IPK homologues in Archaea and the potential importance of this enzyme in isoprenoid metabolism in these organisms, we suggest that these proteins be annotated as isopentenyl phosphate kinases as a distinct group in the AAK superfamily. It seems likely that the fomA gene was acquired by *Streptomyces* via a lateral transfer from Archaea.

ACKNOWLEDGMENT

We thank Dr. Nicole Heaps for samples of IPP. We also thank Dr. James Muller for assistance with mass spectrometry.

SUPPORTING INFORMATION AVAILABLE

Tables of PK homologues and multiple sequence alignments for selected sequences; ^{31}P NMR spectra of reaction mixtures. This material is available free of charge via the Internet at http://pubs.acs.org.

REFERENCES

1. Reiling, K. K., Yoshikuni, Y., Martin, V. J. J., Newman, J., Bohlmann, J., and Keasling, J. D. (2004) Mono and diterpene production in *Escherichia coli*. *Biotechnol. Bioeng. 87*, 200–212.
2. Boucher, Y. (2007) Lipids: biosynthesis, function, and evolution, in Archaea, Molecular and Celluar Biology (Cavicchioli, R., Ed.) pp 341−353, ASM Press, Washington, DC.
3. Boucher, Y., Kamekura, M., and Doolittle, W. F. (2004) Origins and evolution of isoprenoid lipid biosynthesis in archaea. *Mol. Microbiol. 52*, 515–527.
4. Smit, A., and Mushegian, A. (2000) Biosynthesis of isoprenoids via mevalonate in archaea: the lost pathway. *Genome Res. 101*, 1468–1484.
5. Grochowski, L. L., Xu, H. M., and White, R. H. (2006) *Methanocaldococcus jannaschii* uses a modified mevalonate pathway for biosynthesis of isopentenyl diphosphate. *J. Bacteriol. 188*, 3192–3198.
6. Phan, R. M., and Poulter, C. D. (2001) Synthesis of (*S*)-isoprenoid thiodiphosphates as substrates and inhibitors. *J. Org. Chem. 66*, 6705–6710.
7. Keller, R. K., and Thompson, R. (1993) Rapid synthesis of isoprenoid diphosphates and their isolation in one step using either thin layer or flash chromatography. *J. Chromatogr. 645*, 161–167.
8. Davisson, V. J., Woodside, A. B., Neal, T. R., Stremler, K. E., Muehlbacher, M., and Poulter, C. D. (1986) Phosphorylation of isoprenoid alcohols. *J. Org. Chem. 51*, 4768–4779.
9. Zhang, D., and Poulter, C. D. (1993) Biosynthesis of archaebacterial ether lipids. Formation of ether linkages by prenyltransferases. *J. Am. Chem. Soc. 115*, 1270–1277.
10. Duncan, R., and Drueckhammer, D. G. (1993) Phosphorothioate and phosphoramide analogs of dihydroxyacetone phosphate. *Tetrahedron Lett. 34*, 1733–1736.
11. Pilloff, D., Dabovic, K., Romanowski, M. J., Bonanno, J. B., Doherty, M., Burley, S. K., and Leyh, T. S. (2003) The kinetic mechanism of phosphomevalonate kinase. *J. Biol. Chem. 278*, 4510–4515.
12. Cook, P. F., and Cleland, W. W. (2007) Initial velocity studies in the absence of added inhibitors, in Enzyme kinetics and mechanism, pp 59−120, Taylor & Francis Group, LLC, New York.
13. Cook, P. F., and Cleland, W. W. (2007) Enzyme assays, in Enzyme kinetics and mechanism , pp 19−34, Taylor & Francis Group, LLC, New York.
14. Aitken, S. M., Kim, D. H., and Kirsch, J. F. (2003) *Escherichia coli* cystathionine γ-synthase does not obey ping-pong kinetics. Novel continuous assays for the elimination and substitution reactions. *Biochemistry 42*, 11297–11306.
15. Peracchi, A., Bettati, S., Mozzarelli, A., Rossi, G. L., Miles, E. W., and Dunn, M. F. (1996) Allosteric regulation of tryptophan synthase: effects of pH, temperature, and α-subunit ligands on the equilibrium distribution of pyridoxal 5′-phosphate-L-serine intermediates. *Biochemistry 35*, 1872–1880.
16. Gloss, L. M., and Kirsch, J. F. (1995) Use of site-directed mutagenesis and alternative substrates to assign the prototropic groups important to catalysis by *Escherichia coli* aspartate aminotransferase. *Biochemistry 34*, 3999–4007.
17. Cheek, S., Zhang, H., and Grishin, N. V. (2002) Sequence and structure classification of kinases. *J. Mol. Biol. 320*, 855–881.
18. Pakhomova, S., Bartlett, S. G., Augustus, A., Kuzuyama, T., and Newcomer, M. E. (2008) Crystal structure of fosfomycin resistance

kinase FomA from *Streptomyces wedmorensis*. *J. Biol. Chem.* (Epub ahead of print).
19. Marina, A., Alzari, P. M., Bravo, J., Uriarte, M., Barcelona, B., Fita, I., and Rubio, V. (1999) Carbamate kinase: new structural machinery for making carbamoyl phosphate, the common precursor of pyrimidines and arginine. *Protein Sci. 8*, 934–940.
20. Fernandez-Murga, M. L., Gil-Ortiz, F., Llacer, J. L., and Rubio, V. (2004) Arginine biosynthesis in *Thermotoga maritima*: characterization of the arginine-sensitive *N*-acetyl-L-glutamate kinase. *J. Bacteriol. 186*, 6142–6149.
21. Faehnle, C. R., Liu, X., Pavlovsky, A., and Viola, R. E. (2006) The initial step in the archaeal aspartate biosynthetic pathway catalyzed by a monofunctional aspartokinase. *Acta Crystallogr., Sect. F 62*, 962–966.
22. Marco-Marin, C., Ramon-Maiques, S., Tavarez, S., and Rubio, V. (2003) Site-directed mutagenesis of *Escherichia coli* acetylglutamate kinase and aspartokinase III probes the catalytic and substrate-binding mechanisms of these amino acid kinase family enzymes and allows three-dimensional modelling of aspartokinase. *J. Mol. Biol. 334*, 459–476.
23. Ramon-Maiques, S., Marina, A., Gil-Ortiz, F., Fita, I., and Rubio, V. (2002) Structure of acetylglutamate kinase, a key enzyme for arginine biosynthesis and a prototype for the amino acid kinase enzyme family, during catalysis. *Structure 10*, 329–342.
24. Marina, A., Uriarte, M., Barcelona, B., Fresquet, V., Cervera, J., and Rubio, V. (1998) Carbamate kinase from *Enterococcus faecalis* and *Enterococcus faecium*. *Eur. J. Biochem. 253*, 280–291.
25. Huo, X., and Viola, R. E. (1996) Substrate specificity and identification of functional groups of homoserine kinase from *Escherichia coli*. *Biochemistry 35*, 16180–16185.
26. Ward, N. E., and O'Brian, C. A. (1992) The intrinsic ATPase activity of protein kinase C is catalyzed at the active site of the enzyme. *Biochemistry 31*, 5905–5911.
27. Mendelow, M., Prorok, M., Salerno, A., and Lawrence, D. S. (1993) ATPase-promoting dead end inhibitors of the cAMP-dependent protein kinase. *J. Biol. Chem. 268*, 12289–12296.
28. Paudel, H. K., and Carlson, G. M. (1991) The ATPase activity of phosphorylase kinase is regulated in parallel with its protein kinase activity. *J. Biol. Chem. 266*, 16524–16529.
29. Chen, G., Porter, M. D., Bristol, J. R., Fitzgibbon, M. J., and Pazhanisamy, S. (2000) Kinetic mechanism of the p38-α MAP kinase: phosphoryl transfer to synthetic peptides. *Biochemistry 39*, 2079–2087.
30. Knowles, J. R. (1980) Enzyme-catalyzed phosphoryl transfer reactions. *Annu. Rev. Biochem. 49*, 877–919.
31. O'Brian, C. A., and Ward, N. E. (1990) Characterization of a calcium- and phospholipid-dependent ATPase reaction catalyzed by rat brain protein kinase C. *Biochemistry 29*, 4278–4282.
32. Pandey, V. N., and Pradhan, D. S. (1981) Reverse and forward reactions of carbamyl phosphokinase from *Streptococcus faecalis* R. Participation of nucleotides and reaction mechanisms. *Biochim. Biophys. Acta 660*, 284–292.
33. Manca de Nadra, M. C., Pesce de Ruiz Holgado, A. A., and Oliver, G. (1987) Carbamate kinase of *Lactobacillus buchneri* NCDO110. II. Kinetic studies and reaction mechanism. *Biotechnol. Appl. Biochem. 9*, 141–145.
34. McKay, G., and Shargool, P. (1981) Purification and characterization of N-acetylglutamate 5-phosphotransferase from pea (*Pisum sativum*) cotyledons. *Biochem. J. 195*, 71–81.
35. Dotson, S. B., Somers, D. A., and Gengenbach, B. G. (1990) Kinetic studies of lysine-sensitive aspartate kinase purified from maize suspension cultures. *Plant Physiol. 93*, 98–104.
36. Shaw, J. F., and Smith, W. G. (1977) Studies on the kinetic mechansim of lysine-sensitive aspartokinase. *J. Biol. Chem. 252*, 5304–5309.
37. Kumler, W. D., and Eiler, J. J. (1943) The acid strength of mono and diesters of phosphoric acid. The n-alkyl esters from methyl to butyl, the esters of biological importance, and the natural guanidine phosphoric acids. *J. Am. Chem. Soc. 65*, 2355–2361.
38. Cornish-Bowden, A. (2004) Effect of pH on enzyme activity, in Fundamentals of enzyme kinetics , pp 213−228, Portland Press Ltd., London, U.K.